Journal of the European Ceramic Society **17** (1997) 299–308

PII: S0955-2219(96)00131-8
0955-2219/97/$17.00

Tape-Cast Alumina–Zirconia Laminates: Processing and Mechanical Properties

T. Chartier & T. Rouxel

LMCTS, URA CNRS 320, ENSCI, 47 Av. Albert Thomas, 87065 Limoges Cedex, France

(Received 15 September 1995; revised version received 19 June 1996; accepted 15 July 1996)

Abstract

Alumina–zirconia laminar ceramics made from layers of different compositions with different stacking sequences were fabricated by tape casting and compared. A phosphate ester dispersant was optimized in MEK/EtOH and an optimum formulation of organic components for tape casting was defined. The fracture resistance, toughness and elastic properties were characterized. A significant improvement of both the fracture resistance and the toughness, from 380 to 560 MPa and from 3·7 to 8 MPa$\sqrt{m}$ respectively, was gained between the pressed alumina monolith and the tape-cast Al_2O_3–ZrO_2 composites. The improvement was tentatively related to the presence of residual stresses at both the microscopic scale (phase transformation toughening) and at the macroscopic scale (interface effects). © *1996 Elsevier Science Limited.*

1 Introduction

Engineering applications require improved mechanical properties of ceramics, particularly fracture toughness. A noticeable increase in toughness can be obtained through ceramic composites. At the microscopic scale, composites can be roughly classified into particle-, platelet- and whisker-reinforced materials. At the macroscopic scale, composite materials can be arranged according to various configurations, among which are laminated composites, consisting of alternate layers with different compositions. These structures provide the opportunity for tailoring the properties by stacking layers of different compositions in a suitable sequence. It is then possible to produce functionally gradient ceramics to meet specific requirements.[1–9]

The laminated ceramic composites which are studied here consist of alternate layers of alumina reinforced by various amount of zirconia.[10] The aim is to improve both the toughness and the strength. This type of composite allows the association of two reinforcing mechanisms, the first acting at the scale of the microstructure, inside the layers, due to the stress-induced transformation of zirconia particles, the second acting at a macroscopic scale, due to the interfaces between the layers. In these laminar structures, residual stresses develop during cooling from the sintering temperature because of the differences in thermal expansions between layers of different compositions. The sign and the magnitude of these stresses may be adjusted through the compositions, the stacking sequences, and also through the layer thicknesses. Hence, it is possible to develop high compressive stresses in thin layers whereas the tensile stresses remain low in the associated thick layers.

Tape casting,[11–14] which is extensively used for electronic ceramics, is well suited to fabricate homogeneous wide and thin ceramic sheets that can be reinforced by zirconia particles. Multilayer systems are made by stacking green sheets, laminating, removing the organic components and sintering. Tape casting involves the dispersion of the ceramic powder in a solvent (typically organic) with the aid of a dispersant, followed by the addition of binders and plasticizers to ensure the cohesion, flexibility and workability of the green tape when the solvent is evaporated.

This paper describes the processing of laminated Al_2O_3–ZrO_2 composites by tape casting and the optimization of the dispersion which is a crucial step. The influence of organic compounds on properties of green tapes, cracking sensitivity, density and thermocompression ability will also be reported. The room temperature fracture characteristics (strength, toughness, fracture path) and elastic properties were investigated to give an insight into the complex nature of the mechanical behaviour of ceramic laminates and to illustrate the advantages of the composite materials over monoliths.

2 Experimental Procedure

2.1 Starting materials

Tape casting slurries are complex, multicomponent systems, which contain ceramic powders (including sintering aids), solvents, dispersants, binders and plasticizers. The starting powders are 99·7 wt% purity, 0·5 μm grain size alumina (P172SB, Péchiney, France) and 97·5 wt% purity, 0·4 μm grain size zirconia (UPH 12, Criceram, France).

Tape casting slurries were prepared with an azeotropic mixture of methyl ethyl ketone (MEK) and ethanol (EtOH) (40/60 vol%), which is a rather low polarity solvent (dielectric constant = 20). The use of an efficient dispersant is necessary to obtain an homogeneous and stable dispersion of ceramic particles in the solvent, and to achieve a low viscosity with a high ceramic/organic ratio. A stable dispersion of deagglomerated particles leads to a dense particle packing and to an homogeneous microstructure. According to previous studies,[15–18] phosphate esters were chosen to disperse Al_2O_3 and ZrO_2 powders in the MEK/EtOH solvent. The effectiveness of different phosphate esters was evaluated using the viscosity of the ceramic/dispersant/solvent systems.

The binder used is a polyvinyl butyral (PVB) and the plasticizer a mixture of polyethylene glycol (PEG) and dibutyl phthalate (DBP).

2.2 Slurry preparation

The preparation of slurries is carried out in two stages, namely (i) the deagglomeration and dispersion of powders in the solvent with the aid of the dispersant, and (ii) the homogenization of the slurry with binders and plasticizers. The sequence of component addition is critical. The dispersant has to be added before the binders to prevent competitive adsorption.[17] The initial adsorption of the binder on the particle surfaces would prevent the dispersant from being adsorbed subsequently, thereby decreasing its effectiveness. Furthermore, the deagglomeration is more efficient in a low-viscosity system (i.e. without binders and plasticizers) and the mechanical damage of the binder molecules is minimized by this sequence of addition. The deagglomeration is carried out by ultrasonic treatment.[19] The second stage of homogenization is performed by milling for 24 h. The slurry is rotated continuously at a slow speed for de-aeration and to prevent settling.

All the organic components affect the rheological behaviour of the slurry and therefore affect the properties of the green tapes. An optimized slurry should lead to tapes which satisfy the following criteria: (i) no cracking during drying, (ii) high green density, (iii) good microstructural homogeneity, and (iv) good thermocompression ability. Two parameters were chosen to improve the slurry composition with regards to the crack sensitivity, density and thermocompression ability of the green tapes. The first is the volume solids ratio (X = vol% solids = powder/powder + dispersant + binder + plasticizer) and the second is the volume binder to plasticizer ratio (Y = binder/plasticizer). Alumina+10 vol% zirconia slurries were prepared and tape cast with volume solids values varying from 0·6 to 0·9 with steps of 0·05 and binder/plasticizer values varying from 0·3 to 1·9 with steps of 0·4. In all cases, the viscosities of slurries were adjusted to 1 Pa s by addition of solvent.

2.3 Tape casting

Tape casting was performed with a laboratory tape casting bench (Cerlim Equipement, Limoges, France). Slurries were tape cast onto a fixed glass plate with a moving double blade device at a constant speed of 1 m min^{-1}. The thickness of the green tapes was 160 μm.

2.4 Processing of alumina–zirconia laminar composites

Laminar composites consisting of stacked layers of alumina with various zirconia contents (Al_2O_3 = A, Al_2O_3 + 5 vol% ZrO_2 = AZ5, Al_2O_3 + 10 vol% ZrO_2 = AZ10) were fabricated by thermocompression, pyrolysis of the organic components and sintering. Two series of composites were prepared by thermocompression of 19 to 22 single layers of different compositions with different stacking sequences. The number of layers depends on the stacking sequence. The first series is devoted to the influence of the processing routes, transformation toughening and interfacial effects. The second series consists of composites of A and AZ10 layers with different stacking sequences. Both series are designed according to the schematic drawings of Fig. 1. A/A, AZ5/AZ5 and AZ10/AZ10 are not true laminar composites; however these materials were fabricated for comparison with the properties of laminar composites and with monolithic materials prepared by dry pressing (i.e. A and AZ10).

The thermocompression was performed at 110°C under a pressure of 60 MPa.

2.5 Pyrolysis and sintering

Thermal debinding remains one of the most critical steps of ceramic processing and requires an efficient heating cycle to prevent stresses and the formation of defects in ceramic parts. According to the thermogravimetric analysis of tape-cast

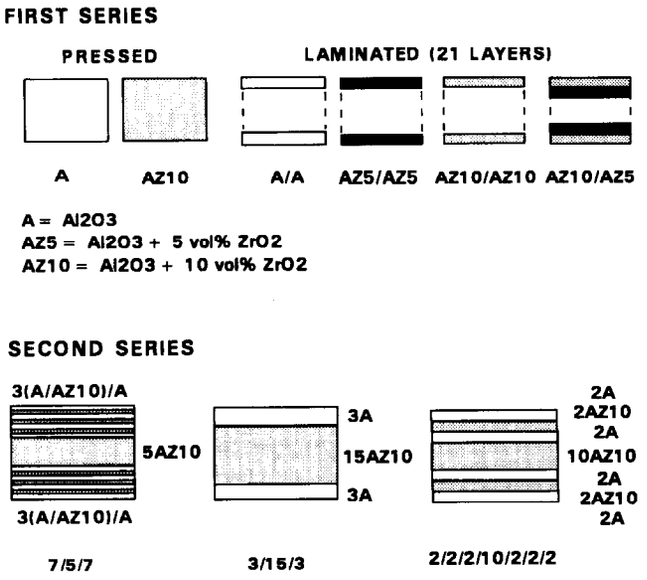

Fig. 1. Schematics of the two series of laminar composites tested.

samples, the pyrolysis was carried out with heating at rate of 1°C min^{-1} up to 120°C, then with heating at rate of 0·1°C min^{-1} up to 550°C with a dwell time of 4 h. The samples were sintered in an electric furnace with $MoSi_2$ heating elements, with heating at rate of 5°C min^{-1} up to 1600°C with a dwell time of 3 h.

2.6 Characterization

Rheological measurements were performed using a rotating cylinder viscometer (Rotovisco RV12, Haake) at a shear rate of 28 s^{-1}. The shear rate was evaluated according to the gap between the casting support and the moving blade, and to the casting speed.

The apparent densities of green samples, excluding organic phases, were determined by measuring the volume (V) and weight ($M_{cal.}$) of samples before and after calcination, respectively. The apparent density is expressed by the $M_{cal.}/V$ ratio.

Evaporation of solvent can cause visible cracking of tapes. The tape shrinkage, and then the shrinkage rate, during drying were measured by a laboratory-made detector using a laser system.[20]

The presence of any delaminations between layers in the green composite was detected using an ultrasonic method.[2]

The mechanical testing was conducted in bending on an INSTRON 8562 testing machine equipped with a differential measurement device, by means of a Linear Variable Displacement Transducer (LVDT) and mechanical contact with the specimen, to accurately measure the specimen deflection. Fracture tests were performed in three-point bending, on 3 × 4 × 25 mm (height × width × length) rectangular bars with a 20 mm

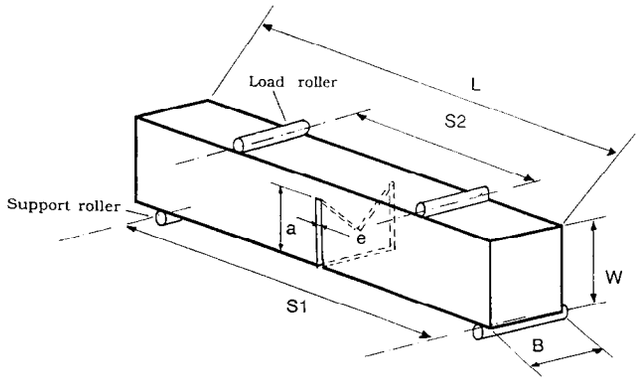

Fig. 2. Chevron-notched (CN) specimens used for the fracture toughness and fracture energy determinations.

span length and a cross-head speed of 0·1 mm min^{-1}. The toughness was measured by four-point bending of 4 × 3 × 50 mm (height × width × length) chevron-notched (CN) specimens (Fig. 2), with a 60° V-notch angle, and a 0·15 mm notch width, inner and outer span of 20 and 40 mm respectively, and cross-head speeds between 0·001 and 0·1 mm min^{-1}. The V-notch is cut perpendicular to the laminae. However, two different orientations of the V, relative to the orientation of the laminae, were investigated to make the crack propagate normal to the layers (N specimens) or transverse to them (T specimens). The mode I fracture toughness K_{IC} is then calculated from the maximum load measured on the experimental curves, using the polynomial equation of Munz *et al.*[21] Chevron-notched specimens were used because of their suitability for fracture toughness determination in brittle materials. Sharpness of the notch is not critical and in the absence of the R-curve effect, K_{IC} values are relatively independent of the initial crack length and agree with the values obtained from straight-through crack specimens with notch thickness as low as 66 μm (single edge notched beam specimens).[21] The elastic moduli were measured by means of an ultrasonic technique, using 10 MHz piezo-electric transducers in contact with specimens. Young's modulus (E) and the shear modulus (G) are calculated from the measured values for the compressional (V_c) and shear (V_s) wave velocities according to:[22]

$$E = \rho \frac{(3V_c^2 - 4V_s^2)}{\left(\frac{V_c}{V_s}\right)^2 - 1} \quad \text{and} \quad G = \rho V_s^2 \qquad (1)$$

where ρ is the specific mass, as measured by Archimedes method using distilled water. Poisson's ratio (ν) is then given by:[23]

$$\nu = \frac{E}{2G} - 1 \qquad (2)$$

3 Results and Discussion

3.1 Tape casting of layers

3.1.1 Selection of the parameters of phosphate esters

The effectiveness of the different phosphate esters was evaluated using the viscosity of the alumina/dispersant/solvent systems. The phosphate esters used were prepared by reaction between phosphoric acid and an ethoxylate. The ethoxylate is obtained by condensation of ethylene oxide in alcohol. The esters contain a combination of mono- and diesters and the remains of the ethoxylate not combined with the phosphoric acid. The chemical structure of a typical phosphate ester is shown in Fig. 3. The influence of four parameters was studied, namely (i) the molecular structure (aliphatic or aromatic),[15] (ii) the monoester/diester ratio, (iii) the degree of phosphatization, and (iv) the Hydrophile/Lipophile Balance (HLB). The addition of phosphate ester to alumina results in lowering the pH, indicating that the dispersant partially dissociates. Without phosphate ester, the alumina powder exhibited a slightly negative surface charge in MEK/EtOH. The surface reversed to positive after addition of phosphate ester suggesting that the H^+ ions liberated on dissociation were adsorbed onto alumina particles. Phosphate esters act by a combination of electrostatic and steric repulsion. The steric hindrance prevents contact between particles. The double layer, which may be due to net charge on the particle surface and/or charges coming from the dissociation of the adsorbed polymer, provides repulsion by a potential energy barrier at larger distances.

The best dispersion (i.e. the lowest viscosity) is achieved with a phosphate ester having (i) an aliphatic molecule, (ii) a high diester concentration, as diesters contain two lipophilic tails, each able to extend into the solvent for steric stabilization, (iii) a high degree of phosphatization because

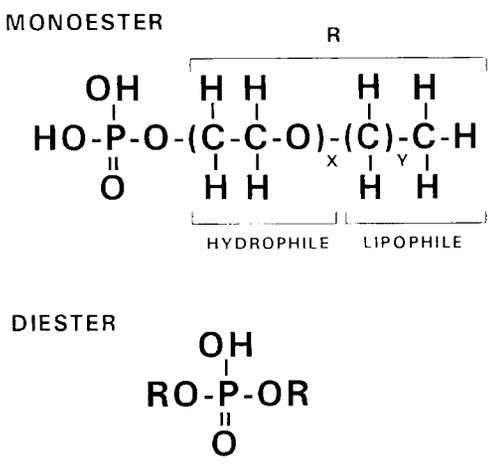

Fig. 3. Typical chemical structure of a phosphate ester.

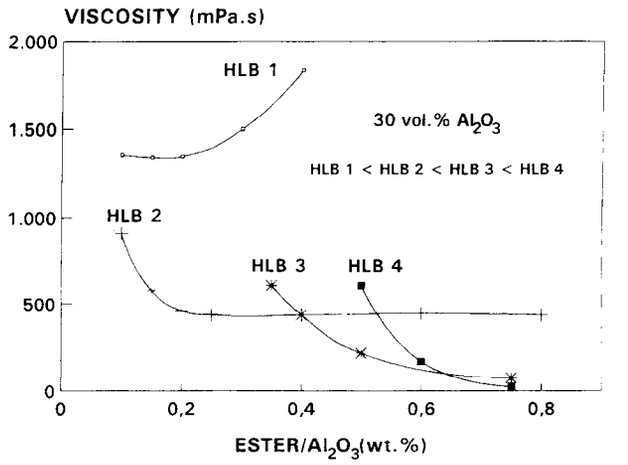

Fig. 4. Apparent viscosity of a 30 vol% alumina suspension versus dispersant concentration for phosphate esters with different HLB values.

the unreacted ethoxylate disturbs ceramic/dispersant interactions and increases the viscosity, and (iv) a high HLB because adsorption on charged ceramic particles is favoured by more hydrophilic dispersants (Fig. 4).

The most efficient phosphate ester, fulfilling all these characteristics, was synthesized and commercialized (Beycostat C213, CECA, France).[15]

3.1.2 Selection of the slurry formulation

For Al_2O_3+10 vol% ZrO_2 green sheets, cracking develops for a volume solids ratio (X) higher than 0·75 and for a binder/plasticizer ratio (Y) higher than 0·7 (Table 1). Cracking depends on shrinkage rate, which depends itself on the composition of the slurry. The maximum shrinkage rate decreases when the volume solids ratio decreases. The high content of organic phase slows down the motion of particles, then reduces the shrinkage rate.

Binders are polymeric molecules which adsorb on the particle surfaces and form organic bridges

Table 1. Cracking during drying (C.: cracking, N.C.: non-cracking) and green density, excluding the organic phase, of alumina+10 vol% zirconia tapes (theoretical density = 4·19 g cm^{-3}) for various values of X and Y

	Composition		*Cracking*	*Green density (g cm^{-3})*
	X	Y		
X1	0·6	0·7	N.C.	2·28
X3	0·7	0·7	N.C.	2·48
X4	0·75	0·7	N.C.	2·52
<=	CRACKING LIMIT			=>
X5	0·8	0·7	C.	2·56
X7	0·9	0·7	C.	2·60
Y1	0·7	0·3	N.C.	2·64
Y2	0·7	0·7	N.C.	2·48
<=	CRACKING LIMIT			=>
Y3	0·7	1·1	C.	2·45
Y4	0·7	1·5	C.	2·43
Y5	0·7	1·9	C.	2·40

Table 2. Composition of the retained tape casting slurry

Component	*Function*	*Vol%*
Alumina + Zirconia	Ceramic powder	30·6
MEK/ethanol	Solvent	57·6
Phosphate ester	Dispersant	0·8
PVB	Binder	4·6
PEG 300	Plasticizer	2·9
DBP	Plasticizer	3·5

between them. The shrinkage rate increases when the binder/plasticizer ratio increases because the high binder content increases the links between particles and then the shrinkage rate. In order to avoid cracking during drying, the formulation of the slurry has to be defined to achieve a low shrinkage rate, i.e. with a high amount of plasticizer-rich organic phase. In the case of the AZ10 system, the shrinkage rate does not exceed a value of 1 $\mu m\ s^{-1}$.

The apparent densities of dried tapes, excluding the organic phase, were determined for various volume solids and binder/plasticizer ratios. When the volume solids ratio decreases, the organic phase prevent particles from packing together, therefore the density decreases. A low binder/plasticizer ratio leads to green tapes with higher densities. When the binder/plasticizer ratio decreases, the low-viscosity plasticizer-rich organic phase allows a good packing of ceramic particles.

3.1.3 Thermocompression ability

The thermocompression behaviour of green sheets is sensitive to *X* and *Y*. Delaminations were numerous in samples with low quantities of organic phases (X4 to X7) (Table 1). A lot of delaminations were observed in samples with a high quantity of plasticizer (Y1). Plasticizers are low molecular weight species which can act as a lubricant between the individual layers, limiting the bond strength during thermocompression.

The final formulation of tape casting slurries was defined in order to tape cast non-cracked tapes with a high green density, which do not lead to delamination during thermocompression of laminated composites. This formulation (Table 2) was applied to the tape casting of pure alumina and of Al_2O_3+5 vol% ZrO_2 with similar green tape characteristics and a good thermocompression ability.

3.2 Laminar composites

3.2.1 Design

Some physical properties of monoliths and composites are given in Table 3. These physical properties were used to design the composites in such a

Table 3. Physical properties of the various grades tested. *E* and *G* are measured normal to the direction of the layering. Poisson's ratio is equal to 0·24 for all the grades

Material	E *(GPa)*	G *(GPa)*	$\alpha_{20\ 1400°C}$ *(10^6 °C^{-1})*
A	355	143	8·69
A/A	363	146	—
AZ10	341	137	8·80
AZ5/AZ5	349	141	9·06
AZ10/AZ10	342	138	—
AZ10/AZ5	—	—	—
7/5/7	362	146	—
3/15/3	349	141	—
2/2/2/10/2/2/2	377	152	—

way that compressive residual stresses develop in the outer layers. These residual stresses were induced upon cooling from high temperature (1400°C), as a result of different thermal expansion coefficients between the layers. The classical plate theory (plane stress hypothesis) was used to calculate the normal stresses in each layer of the two-phase composite.[24] In its main lines, the calculation is based on the assumption that a cross-section before deformation remains a cross-section after deformation and that layers remain plane and parallel to each other throughout deformation. This results in the following form for the elastic displacement vector at any point (x_1, x_2, x_3):

$$\vec{u} = \begin{cases} u_1 = u_1^0(x_1, x_2) \\ u_2 = u_2^0(x_1, x_2) \\ u_3 = u_3^0(x_3) \end{cases} \tag{3}$$

where (1,2) subscripts refer to the in-plane axis and (3) is normal to the layering. The studied laminates are constructed such that they have complete symmetry of individual lamina thickness and properties about the middle plane of the laminate. Furthermore, no texture was introduced by the tape casting process, so that the studied laminates can be considered as perfectly orthotropic. Hence, in the case of pure linear elasticity, the thermally induced normal (N_1 and N_2) and tangential (T_{12}) forces, per unit length, are given by:[24]

$$\begin{bmatrix} N_1 \\ N_2 \\ T_{12} \end{bmatrix} = \begin{bmatrix} A_{11} & A_{12} & 0 \\ A_{21} & A_{22} & 0 \\ 0 & 0 & A_{66} \end{bmatrix} \begin{bmatrix} \varepsilon_{11} \\ \varepsilon_{22} \\ \varepsilon_{12} \end{bmatrix} \tag{4}$$

with $A_{11} = \dfrac{Ed}{1-\nu^2}$, $A_{12} = A_{21} = \dfrac{\nu Ed}{1-\nu^2}$, $A_{66} = 2Gd$

and $\varepsilon_{ij} = \dfrac{1}{2}\left[\dfrac{\partial u_i}{\partial x_j} + \dfrac{\partial u_j}{\partial x_i}\right]$.

One recalls that eqns (4) only stand for the elastic part of the strain components ($\varepsilon^{\text{elastic}} = \varepsilon^{\text{total}} - \varepsilon^{\text{thermal}}$),

so that the normal force N_1^I in a layer of composition (I) is expressed by :

$$N_1^I = A_{11}^I (\varepsilon_{11}^I - \alpha^I \Delta T) + A_{12}^I (\varepsilon_{12}^I - \alpha^I \Delta T) \quad (5)$$

where α^I is the isotropic thermal expansion coefficient of material (I).

In the absence of external forces, (1) and (2) are equivalent axes and $\varepsilon_{11} = \varepsilon_{22}$:

$$N_1^I = (A_{11}^I + A_{12}^I)(\varepsilon_{11}^I - \alpha^I \Delta T) \quad (6)$$

The overall equilibrium of the system in the (1) direction gives, for a composite consisting of n layers of composition (I) and p layers of composition (II):

$$nN_1^I + pN_1^{II} = 0 \quad (7)$$

u_1 being independent of x_3, so are ε_{11} and σ_{11}. This allows N_1 to be expressed as a function of σ_{11}:

$$N_1 = \int_0^d \sigma_{11} dx_3 = \sigma_{11} d \quad (8)$$

Substituting in eqn (7) gives:

$$n\sigma_{11}^I d^I + p\sigma_{11}^{II} d^{II} = 0 \quad (9)$$

It is further assumed that a perfect interfacial bonding exists between the layers, so an additional kinematic hypothesis is now considered: $u_1^I = u_1^{II}$, and since the laminates consist of layers of identical length and width, it becomes: $\varepsilon_{11}^I = \varepsilon_{11}^{II}$. Extracting the strain from eqn (6) and taking eqn (8) for the normal force expression gives the following boundary condition:

$$\frac{\sigma_{11}^I d^I}{A_{11}^I + A_{12}^I} + \alpha^I \Delta T = \frac{\sigma_{11}^{II} d^{II}}{A_{11}^{II} + A_{11}^{II}} + \alpha^{II} \Delta T \quad (10)$$

By writing eqns (9) and (10) for each of the laminate composites, it is possible to calculate the normal residual stresses in the various layers of the composite. For instance, in the case of the 2/2/2/10/2/2/2 grade, otherwise modelled by a IV/III/II/I/II/III/IV sequence, the following set of equations is obtained:

Three boundary conditions

$$\left(\frac{1-\nu^I}{E^I}\right)\sigma_{11}^I + \alpha^I \Delta T = \left(\frac{1-\nu^{II}}{E^{II}}\right)\sigma_{11}^{II} + \alpha^{II} \Delta T$$

$$\left(\frac{1-\nu^{II}}{E^{II}}\right)\sigma_{11}^{II} + \alpha^{II} \Delta T = \left(\frac{1-\nu^I}{E^I}\right)\sigma_{11}^{III} + \alpha^I \Delta T \quad (11)$$

$$\left(\frac{1-\nu^I}{E^I}\right)\sigma_{11}^{III} + \alpha^I \Delta T = \left(\frac{1-\nu^{II}}{E^{II}}\right)\sigma_{11}^{IV} + \alpha^{II} \Delta T$$

One equilibrium equation

$$5\sigma_{11}^I + 2(\sigma_{11}^{II} + \sigma_{11}^{III} + \sigma_{11}^{IV}) = 0 \quad (12)$$

This gives from the data of Table 3: $\sigma_{11}^I = \sigma_{11}^{III} = 28$ MPa and $\sigma_{11}^{II} = \sigma_{11}^{IV} = -49$ MPa.

Table 4. Calculated values for the residual stresses in the inner and outer layers of the two-phase composites

	AZ10/AZ5	*7/5/7*	*3/15/3*	*2/2/2/10/2/2/2*
$\sigma_{11\ \text{outer}}$ (MPa)	−118	−40	−50	49
$\sigma_{11\ \text{inner}}$ (MPa)	130	29	20	28

Results of this first-order calculation are summarized in Table 4. According to the observations, the most questionable hypothesis of the model consists in taking u_1 as a function of (x_1, x_2), that the laminate sides did not form flat surfaces after cooling from the joining temperature, hence that shear strains and stresses (ε_{13} and σ_{13}) develop upon cooling. Estimation of shear effects is currently under survey.

3.2.2 Mechanical properties

The A/A material without interface shows better mechanical properties (σ_r = 408 MPa, K_{IC} = 5·5 MPa$\sqrt{m}$), compared to the same alumina sintered in the same conditions but prepared by dry pressing (σ_r = 380 MPa, K_{IC} = 4·5 MPa$\sqrt{m}$) (Figs 5a

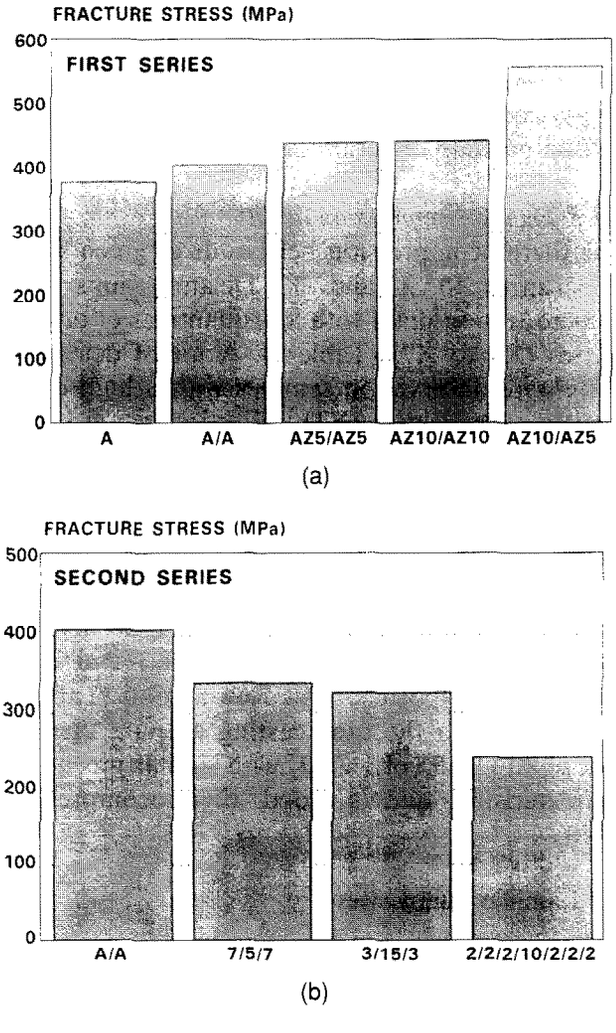

Fig. 5. Fracture resistance (3-point bend test) of the composites from, (a) the first series (b) the second series.

and 9a). This suggests that tape casting leads to a more homogeneous green state, with small compaction defects.

The fracture resistance (σ_r) of both series increases with the zirconia content (Fig. 5). A further improvement is achieved by combining AZ10 and AZ5 layers, probably due to interfacial stresses in this latter case. Curiously, materials from the second series show lower fracture resistances than pure alumina (Fig. 5b). The propagating crack is deflected several times in or near layer interfaces for composite materials (Fig. 6).

Results of the CN tests are depicted in Fig. 7. Figure 7a shows the load/deflection curves obtained on the A, A/A and AZ10/AZ10 with a deflection rate of 0·01 mm min^{-1} together with results obtained on the AZ10/AZ10 with different deflection rates. A and A/A curves are almost superimposed; these materials exhibit unstable crack propagation. A/A fractured specimens show a flat fracture path, essentially transgranular, whereas AZ10/AZ10 specimens fractured with a mixed transgranular/ intergranular path giving rise to a rough fracture surface, as shown in Fig. 8. Stable or semi-stable crack propagations were observed in this latter case, with a significant influence of the cross-head speed on the maximum load peak, i.e. the lower the displacement rate, the higher the fracture toughness. This behaviour is tentatively attributed to the occurrence of crack tip healing processes (blunting) at relatively low testing rates. In conjunction, the work of fracture becomes larger and larger as the testing rate decreases.

Works of fracture (WOF) of $1{\cdot}9 \times 10^{-4}$, $2{\cdot}2 \times 10^{-4}$ and $4{\cdot}0 \times 10^{-4}$ J were determined by computing the area below the load-deflection curves corresponding to cross-head speeds of 0·1, 0·01 and 0·001 mm min^{-1}, respectively. An estimation of the intrinsic fracture surface energy (γ_i) can be obtained from the Griffith/Irwin similarity relationship: $\gamma_i = \frac{K_{IC}^2}{2E}$. From our experimental data γ_i equals 10·7, 19 and 25·9 J m^{-2} for cross-head speeds of 0·1, 0·01 and 0·001 mm min^{-1}, respectively. This very simple calculation shows that work of fracture is significantly higher than $2\gamma_i S$ where S is the minimum fracture surface area as defined by the chevron geometry ($S \approx 4{\cdot}7$ mm^2). This would support either the occurrence of viscoplastic energy dissipation, i.e. $\gamma_{effective} > \gamma_i$ and/or crack deflection ($S_{effective} > S$).

FRACTURE PATH AND FRACTURE SURFACE

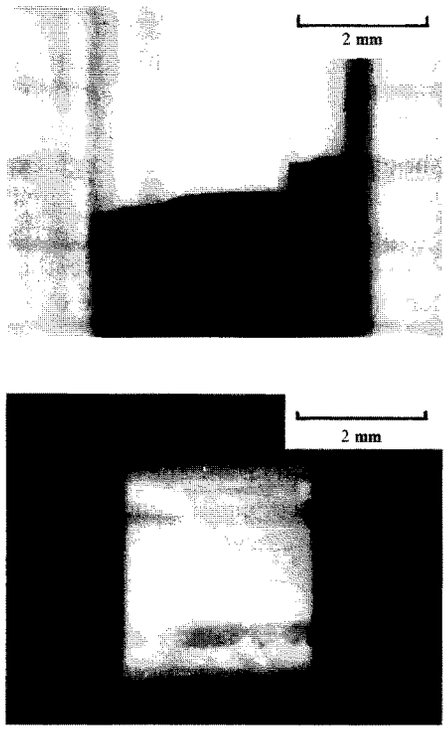

Fig. 6. Fracture path in a 2/2/2/10/2/2/2 specimen fractured in bending.

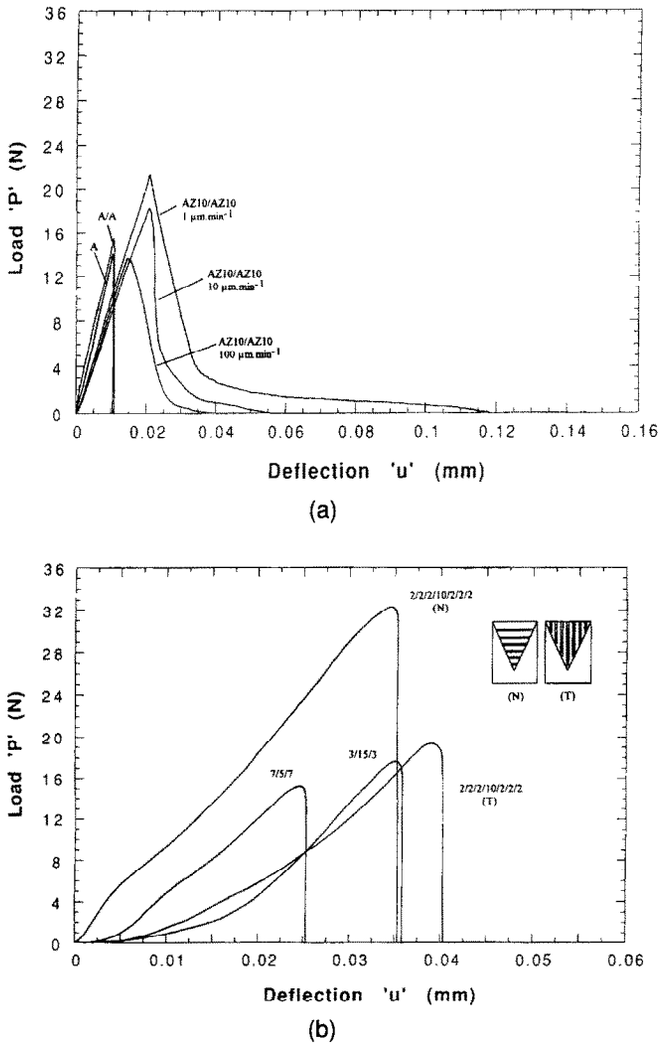

Fig. 7. Chevron notch tests performed in bending on (a) specimens of the AZ10/AZ10 grade with different loading rates and (b) specimens from the second series with a cross-head speed of 10 μm min^{-1} and two layers to crack front orientations in the case of the 2/2/2/10/2/2/2 grade.

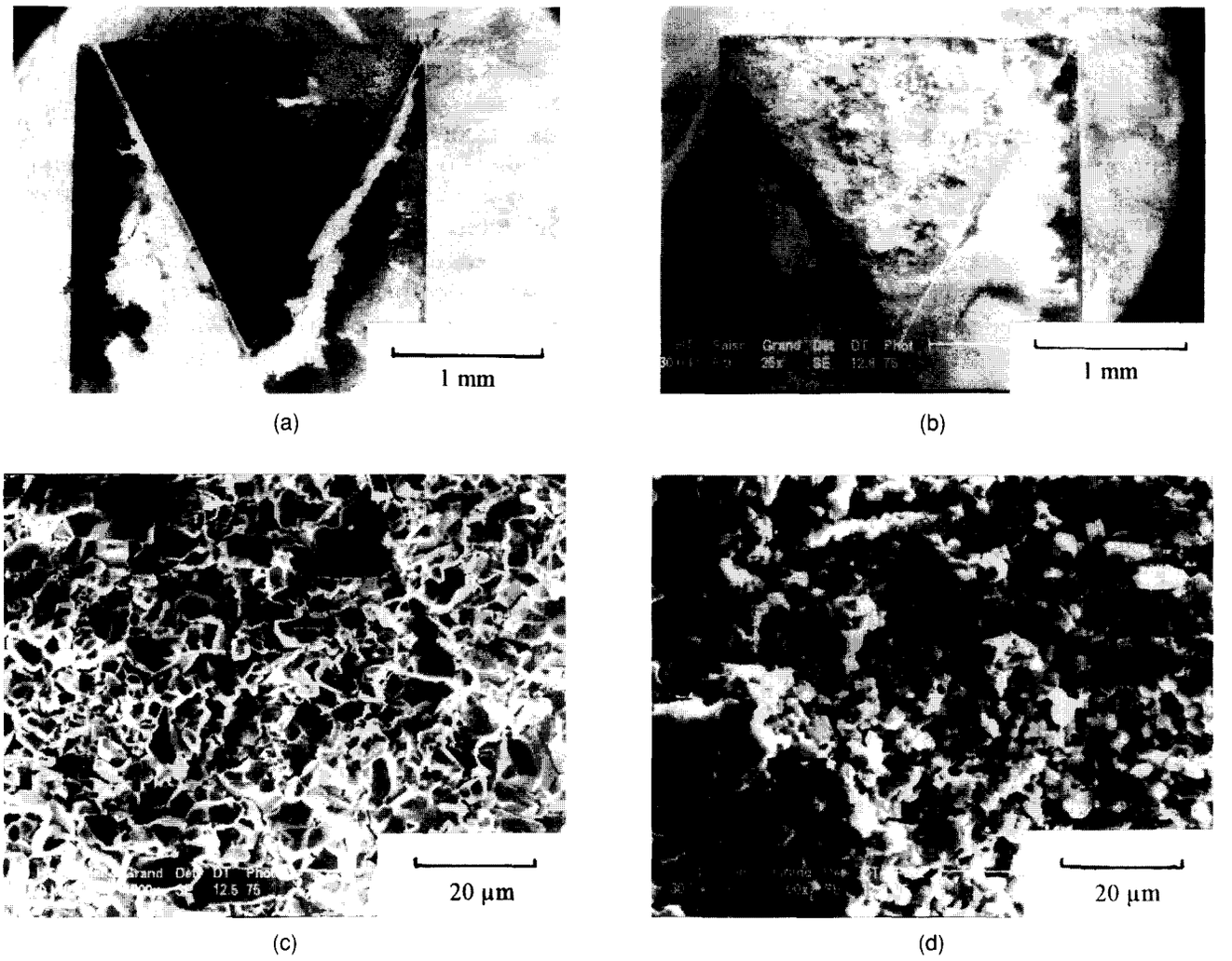

Fig. 8. SEM micrographs of the fracture surfaces from CN specimens of (a) A/A and (b) AZ10/AZ10. Higher magnification views of the fracture path (c) A/A and (d) AZ10/AZ10.

A cross-head speed of 0·01 mm min^{-1} was selected to compare the materials of the second series by Chevron-Notched (CN) tests (Fig. 7b). Under the chosen testing condition, the CN specimens of this series failed in purely brittle mode (unstable crack propagation) with maximum load peaks slightly higher than in the case of AZ10. In addition, the incidence of the layer orientation with respect to the propagation direction was investigated on the 2/2/2/10/2/2/2 grade, by testing a V-notched CN specimen oriented in such a way that the crack propagated parallel to the layer interfaces. This figure shows that the reinforcement is much more significant normal to the layering.

Values for K_{IC} are summarized in Fig. 9, together with the values previously obtained on the same materials by the Single Edge Notched Beam (SENB) method.[2] CN tests give lower values for K_{IC} than SENB tests as is expected. This is tentatively attributed to a sharper crack tip in the first case. Poisson's ratios being identical for all studied materials, the theoretical prediction of Voigt and Reuss (Hill bounds) were drawn from the Young's moduli of A and AZ10 in order to compare with the effective moduli of the different composites (Fig. 10). It is observed that Young's modulus values measured parallel to the layering (which should be close to the Voigt expression) agree well with the prediction, whereas values measured normal to the layering (corresponding to the Reuss model) fall far outside the bounds. This statement confirms the presence of an interfacial effect, affecting the elastic properties, i.e. the ultrasonic wave propagation in the present case. Possible sources for this effect include composition heterogeneities within the layer surfaces (chemical alteration) and changes in the interatomic bonding distances (stored elastic energy or thermally induced residual stresses).

4 Conclusion

Laminar composites proved to have promising mechanical properties with fracture strength and toughness up to 1·5 to 2 times higher for the

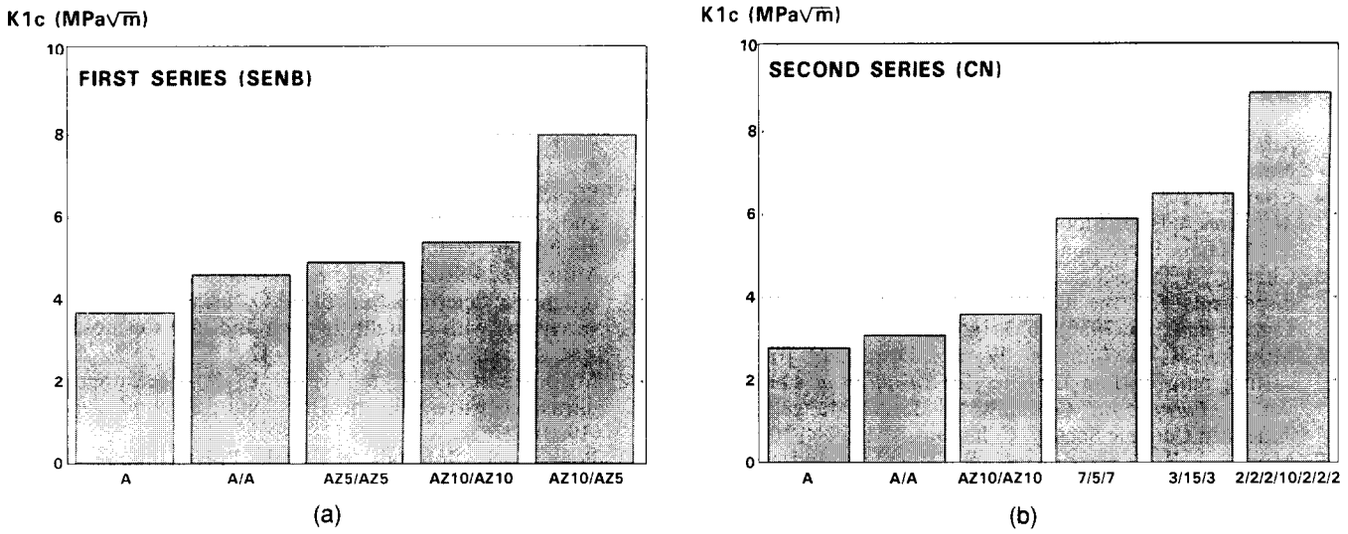

Fig. 9. Fracture toughness of the different grades (a) SENB results from Ref. 2, (b) CN results (cross-head speed = 0·01 mm min $^{-1}$).

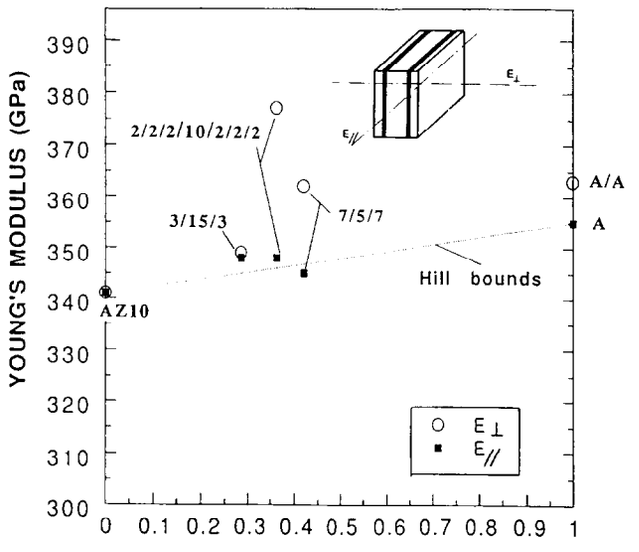

Fig. 10. Young's moduli of the different laminates. The Hill bounds were drawn for comparison. Voigt and Reuss's curves are almost superposed due to rather close Young's moduli for A and AZ10.

composite than for the bulk components. This remarkable improvement is assumed to be essentially related to the presence of thermally induced residual stresses which, according to a simple plane stress model, can be as high as 130 MPa. Crack deflection is essentially a consequence of the residual stresses.

Phosphate esters are highly effective dispersants for alumina in MEK/EtOH solvent, but their effectiveness is strongly dependent on their characteristics. Four parameters were varied and an improved phosphate ester having (i) an aliphatic molecule, (ii) a high diester concentration, (iii) a high degree of phosphatization and (iv) a high Hydrophile/Lypophile Balance was synthesized.

The organic components in a slurry play a prominent role on the green properties of tape-cast materials. The slurry formulation was optimized in order to tape cast defect-free samples with a high green density and a good thermocompression ability.

References

1. Amateau, M. F. & Messing, G. L., Laminated ceramic composites. In *International Encyclopedia of Composites*, vol. 3, ed. S. M. Lee. VCH New York, 1990, pp. 11–16.
2. Chartier, T., Besson, J. L. & Boch, P., Mechanical properties of ZrO_2-Al_2O_3 laminated composites. In *Advances in Ceramics, Science and Technology of Zirconia III*, vol. 24, eds S. Somiya, N. Yamamoto & H. Yanagida. Am. Ceram. Soc., Westerville, Ohio, 1988, pp. 1131–1138.
3. Boch, P., Chartier, T. & Huttepain, M., Tape casting of Al_2O_3/ZrO_2 laminated composites, *J. Am. Ceram. Soc.*, **69**(8) (1986) 191–192.
4. Chartier, T. & Besson, J. L., Behaviour of ZrO_2-Al_2O_3 laminated composites loaded by various mechanical arrangements. In *Science of Ceramics*, vol. 14, ed. D. Taylor. The Institute of Ceramics, UK, 1988, pp. 639–644.
5. Russo, C. J., Harmer, M. P., Chan, H. M. & Miller, G. A. Design of laminated ceramic composite for improved strength and toughness. *J. Am. Ceram. Soc.*, **75**(12) (1992) 3396–3400.
6. Harmer, M. P., Chan, H. M. & Miller, G. A., Unique opportunities for microstructural engineering with duplex and laminar ceramic composites. *J. Am. Ceram. Soc.*, **75**(7) (1992) 1715–1728.
7. Plucknett, K. P., Caceres, C. H. & Wilkinson, D. S., Tape casting of fine alumina/zirconia powders for composite fabrication. *J. Am. Ceram. Soc.*, **77**(8) (1994) 2137–2144.
8. Plucknett, K. P., Caceres, C. H., Hughes, C. & Wilkinson, D. S., Processing of tape-cast laminates prepared from fine alumina/zirconia powders. *J. Am. Ceram. Soc.*, **77**(8) (1994) 2145–2153.
9. Takebe, H. & Morinaga, K., Fabrication and mechanical properties of lamellar Al_2O_3 ceramics. *J. Ceram. Soc. Jpn Inter.*, **96** (1988) 1122–1128.
10. Chartier, T., Merle, D. & Besson, J. L., Laminar ceramic composites. *J. Eur. Ceram. Soc.*, **15** (1995) 101–107.
11. Mistler, R. E., Shanefield, D. J. & Runk, R. B., Tape casting of ceramics. In *Ceramic Processing before Firing*, eds G. Y. Onada & L. L. Hench, John Wiley & Sons, New York, 1978, 411–418.

12. Shanefield, D. J., Tape casting for forming advanced ceramics. In *Encyclopedia of Materials Science and Engineering*, ed. M. B. Bever. 1984, 4855–4858.
13. Williams, J. C., Doctor blade process. In *Treatise on Material Science and Technology*, vol. 9, *Ceramics Fabrication Processes*, ed. F. F. Y. Wang. Academic Press, New York, 1976, 173–197.
14. Chartier, T., Tape casting. In *Encyclopedia of Advanced Materials*, eds D. Bloor, R. J. Brook, M. C. Flemings & S. Mahajan. Pergamon Press, 1994, 2763.
15. Chartier, T., Streicher, E. & Boch, P., Phosphate esters as dispersants for the tape casting of alumina. *J. Am. Ceram. Bull.*, **66** (1987) 1653–1655.
16. Mikeska, K. & Cannon, W. R., Dispersant for tape casting pure barium titanate. In *Advances in Ceramics*, vol. 9, *Forming in Ceramics*, ed J. A. Mangels. The American Ceramic Society, Columbus, OH, 1984, 164–183.
17. Morris, J. R. & Cannon, W. R., Rheology and component interactions in tape casting slurries. In *Materials Research Society Symposium Proceeding*. Mat. Res. Soc. Pittsburgh, PA, USA, **60** (1986) 135–142.
18. MacKinnon, R. J. & Blum, J. B., Particle size distribution effects on tape casting of barium titanate. In *Advances in Ceramics*, vol. 9, *Forming in Ceramics*, ed. J. A. Mangels. 1984, 150–157.
19. Chartier, T., Jorge, E. & Boch, P., Ultrasonic deagglomeration of Al_2O_3 and $BaTiO_3$ for tape casting. *J. Phys. III* (1991) 689.
20. Streicher, E., Chartier, T. & Boch, P., Study of cracking and microstructural evolution during drying of tape-cast aluminium nitride sheets. *J. Mat. Sc.*, **26** (1991) 1659.
21. Munz, D., Bubsey, R. T. & Shannon, J. L. Jr., Fracture toughness determination of Al_2O_3 using four-point-bend specimens with straight-through and chevron notches. *J. Am. Ceram. Soc.*, **63** (1980) 34–42.
22. McSkimmin, H. J. & Fisher, E. S., Measurement of ultrasonic wave velocities for solids. *J. Appl. Phys.*, **31** (1960) 627.
23. Poisson, S., Journal de l'Ecole Polytechnique, Cahier n° 15, 1809, 266.
24. Christensen, R. M., *Mechanics of Composite Materials, Laminates*. Wiley and Sons, New York, 1979, chap. V.